



Assessment of subgrid-scale models for large-eddy simulation of a planar turbulent wall-jet with heat transfer

Priyesh Kakka ^a, Kameswararao Anupindi ^{a,*}

Department of Mechanical Engineering, Indian Institute of Technology Madras, Chennai, T.N. 600 036, India



ARTICLE INFO

Article history:

Received 9 August 2019

Revised 6 February 2020

Accepted 29 February 2020

Keywords:

Large-eddy simulation (LES)

turbulent wall-jet

heat transfer

subgrid-scale (SGS) models

ABSTRACT

In the present work, five different subgrid-scale (SGS) models and implicit large-eddy simulation (LES) are evaluated and compared against the DNS for the simulation of the planar turbulent wall-bounded jet with heat transfer. The SGS models tested are the classical constant coefficient Smagorinsky model and its dynamic version, the wall-adaptive local eddy-viscosity (WALE) model, the turbulent kinetic energy one-equation model, and its dynamic version. The effects of using variable turbulent Prandtl number and the near-wall damping function are also studied in these models. The mean, second-order flow and heat-transfer statistics with the evolution of Nusselt number along the jet downstream are used to assess the different SGS models. The quality of resolution of the present LES are evaluated using the activity parameter and the index of resolution quality. Among the models tested, the constant coefficient Smagorinsky model together with Van-Driest damping predicts the solution accurately in the near-wall region as well as in estimating the thermal parameters. However, the dynamic models performed better in evaluating the Reynolds stress profiles away from the wall in the outer region. Capabilities of the models to predict the turbulent kinetic energy budgets, pressure-velocity gradient correlations and triple velocity correlations are also studied. The implemented variable Prandtl number algorithm is noted to have minimal influence on the evolution of the solution.

© 2020 Elsevier Ltd. All rights reserved.

1. Introduction

The physics of a turbulent jet issued in the vicinity of a wall is quite interesting owing to its inner layer behaving as a turbulent boundary layer and the outer one as a free shear layer. Study of turbulent planar wall-bounded jets is an active area of research because of the interaction between the inner and outer-layers as well as its wide range of applications in electronics cooling, drying, defrosters in cars, and most importantly in the cooling of gas turbine blades. With the advent of modern manufacturing techniques, it is now possible to increase the complexity in the design of gas turbines blades and the combustion chamber liners to enhance film cooling using turbulent wall-jets. Thus there is a need to optimize the flow and heat transfer characteristics for these designs. Such studies require several parameter sweeps and further need a reliable turbulence model that can accurately capture the flow physics.

Several studies in the past employed experimental and numerical techniques to explore wall-bounded jets. A review on the turbulent wall-jets, its modeling and the experiments were done by Launder and Rodi [1,2]. One of the first experiments for wall-jets

was done by Sigalla [3] to find its skin friction coefficient. Akfirat [4] performed experiments and studied a wall-bounded jet for an isothermal boundary condition and obtained a correlation between the Nusselt number (Nu) and the Reynolds number (Re). Mabuchi and Kumadav [5] also reported a similar correlation with different coefficients. Eriksson et al. [6] used laser Doppler velocimetry (LDV) to accurately measure the wall shear stress and the turbulence intensities in a wall-jet for a $Re = 9600$ in the entire flow region. Rostamy et al. [7] conducted experiments using LDV for both smooth and rough walls. AbdulNour et al. [8] experimented with different thermal boundary conditions near the inlet in a region of developing wall-jet for defroster applications. Numerical simulations, with a varying degree of modeling, also exist in the literature that obtained detailed flow physics in a turbulent wall-jet with heat transfer. Using unsteady RANS, Mondal et al. [9] studied the variation in the vortex formation near the inlet due to the interaction of the wall-jet and an offset jet at different height ratios. Kechiche et al. [10] simulated a wall-jet with heat transfer using Reynolds-averaged Navier-Stokes (RANS) based turbulence models and commented on the applicability of different low-Re $k - \epsilon$ models and tuned the coefficients. Rathore and Das [11] compared and demonstrated the accuracy in simulating heat transfer and flow of wall-jet with several RANS models such

* Corresponding author.

E-mail address: kanupindi@iitm.ac.in (K. Anupindi).

Nomenclature

A	activity parameter
C	model coefficients
C_p	specific heat capacity
C_v	convection
D	viscous diffusion
Nu	Nusselt number
Pr	Prandtl number
Re	Reynolds number
S	strain rate tensor
T	temperature
T_d	turbulent diffusion
T_f	friction temperature
U_0	jet inlet velocity
f	frequency
h	jet inlet height
k_f	thermal conductivity of fluid
p	pressure
q	heat flux
t	time
u_τ	friction velocity
y^+	inner-scaled wall normal length
DNS	direct numerical simulation
LDV	laser Doppler velocimetry
LES	large-eddy simulation
LESIQ	LES index of resolution quality
RANS	Reynolds-averaged Navier-Stokes
SGS	subgrid-scale model
WALE	wall-adaptive local eddy-viscosity
i, j, k	free indices
k	total kinetic energy
rms	root mean square
sgs	sub-grid scale quantity
t	turbulent quantity
w	wall
α	thermal diffusivity
Δ	grid size
δ	Kronecker delta
η	wall-normal direction
ν	kinematic viscosity
ϕ	turbulent dissipation
ψ	velocity-pressure gradient correlation
τ	SGS stress tensor
$\langle \phi \rangle$	time averaged quantity
$\bar{\phi}$	filtered quantity
ϕ'	fluctuating quantity
$\hat{\phi}$	test filter

perature variance and the turbulent heat flux were plotted along with different scaling parameters for heat transfer.

With DNS being prohibitively expensive and RANS based simulations not being very accurate, at least in cases involving complex physics, LES emerged as a viable alternative. An exhaustive study of the effect of nozzle configuration on the heat-transfer due to impinging jets was conducted by He et al. [18]. The authors justified comprehensive results and heat-transfer mechanisms based on the physics and characteristics of the flow obtained from the LES results. For the case of wall-jet interacting with the offset jet, Li et al. [19] compared two SGS dynamic models. They found that for the prediction of velocity distribution on the coarser grid, the dynamic k-equation model works better than the modified dynamic Smagorinsky model. Similarly, in the past several studies have been done to test the effectiveness of LES models for natural convection [20], heated impinging-jets [21], twin parallel jets [22], stenotic blood-vessels [23] among others. From the preceding discussion, it can be noted that there are very few studies in the literature that used LES to simulate wall-bounded planar turbulent jets with heat transfer. Further, there are no studies in the literature that evaluated the performance of subgrid-scale (SGS) models for this kind of flows. As noted in the research by Lampitella et al [24], in the simulation of flow over a matrix of cubes, the heat transfer characteristics are very sensitive to the SGS model used. Therefore, the present study aims to assesses the performance of five SGS models and an implicit LES for the simulation of planar turbulent wall-jet with heat transfer. Another contribution of the present work involves the implementation and testing of a variable turbulent Prandtl number in the simulations. The open-source computational fluid dynamics software OpenFOAM [25,26] is used for performing all the simulations.

The remainder of the paper is organized as follows. The equations that govern the present problem, the numerical method used, and the details of the SGS models tested, the geometry, mesh and the boundary conditions are presented in Section 2. The mesh resolution used in the present study is assessed with the help of LES index of resolution quality (LESIQ) are also discussed in this section. In Section 3, the effect of using a variable Prandtl number, effect of the use of Van-Driest damping near the wall, mean, second-order flow and thermal statistics are evaluated. The activity parameter and the iso-surface of Q-criterion are used in order to understand the dissipation of the SGS models and their near-inlet development. The evolution of turbulence kinetic energy budgets, pressure-velocity gradient correlations and the triple velocity correlations are also evaluated for the models considered. Finally, the paper is concluded in Section 4.

2. Governing equations and numerical methods

2.1. Details of the domain and the mesh

The domain, together with the applied boundary conditions is shown in Fig. 1. The inlet of the jet has height h and the mean velocity profile at the inlet is extracted from the DNS studies of Naqavi et al. [16]. With reference to the values from the experiments of Eriksson et al. [6], random fluctuations with an intensity of 1% are superimposed on the mean velocity profile at the inlet to the domain. Further, wall-jets are known to be independent of the inlet conditions in the self-similar region. A non-reflective boundary condition is applied on the outlet of the domain. An impermeable and no-slip boundary condition for velocity is applied on the bottom wall. A weak flow velocity with an intensity of 4% of the maximum inlet velocity is applied on the top boundary in order to aid the entrainment of the fluid into the domain. Dejoan and Leschziner [12] in their study suggest the use of a top wall entrainment velocity that would not affect the dynamics of the jet

as low-Re $k - \epsilon$ model, standard $k - \epsilon$ and the $k - \omega$ SST model. Dejoan and Leschziner [12] performed large-eddy simulation (LES), only for flow without any heat transfer, and studied wall-jet at a Re of 9600. They studied budgets for turbulence energy, Reynolds stresses, and concluded on various processes involved in the interaction between the inner and outer-layer of the wall jets. Similar studies on wall-jets based on roughness and geometry is done by Banyassady and Piomelli [13,14]. Naqavi et al. [15] performed LES for a turbulent wall-jet issued into a hot external stream at different velocity ratios. They studied the heat transfer, flow physics, and the interaction of the two. Further, in a separate study Naqavi et al. [16,17] used direct numerical simulation (DNS) to study the heat transfer characteristics and the flow physics of a turbulent wall jet at a Re of 7500 by employing a grid resolution of 172 million cells. Through this study they reported the budgets for tem-

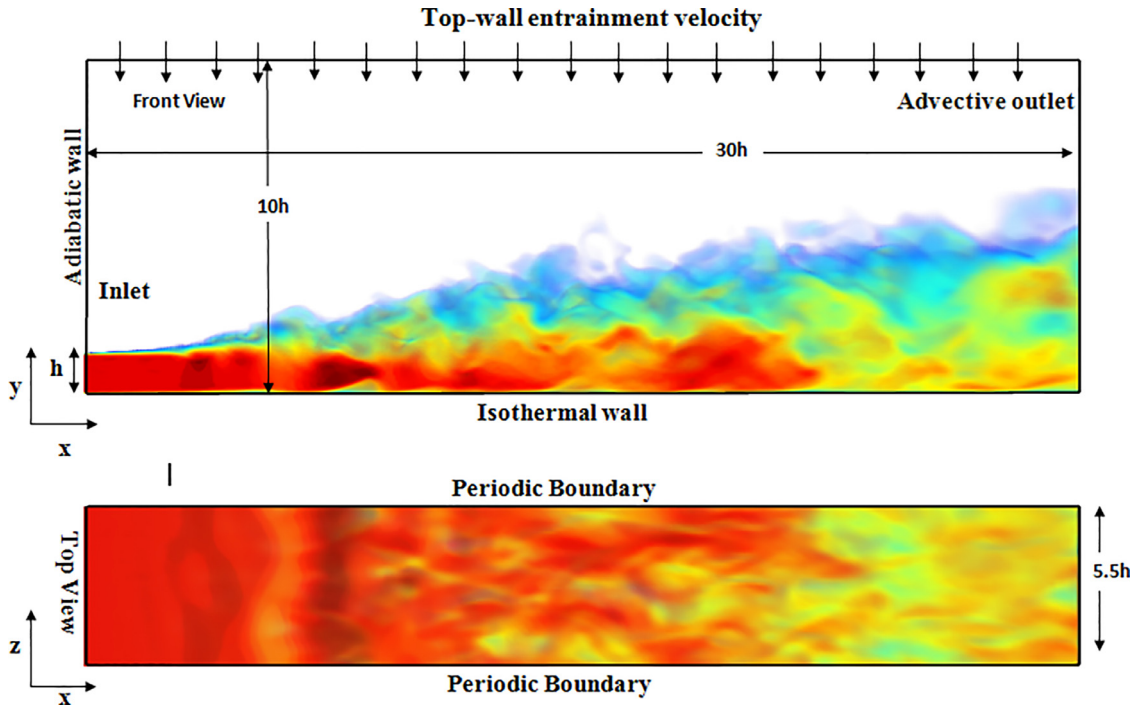


Fig. 1. Schematic of the domain together with the applied boundary conditions.

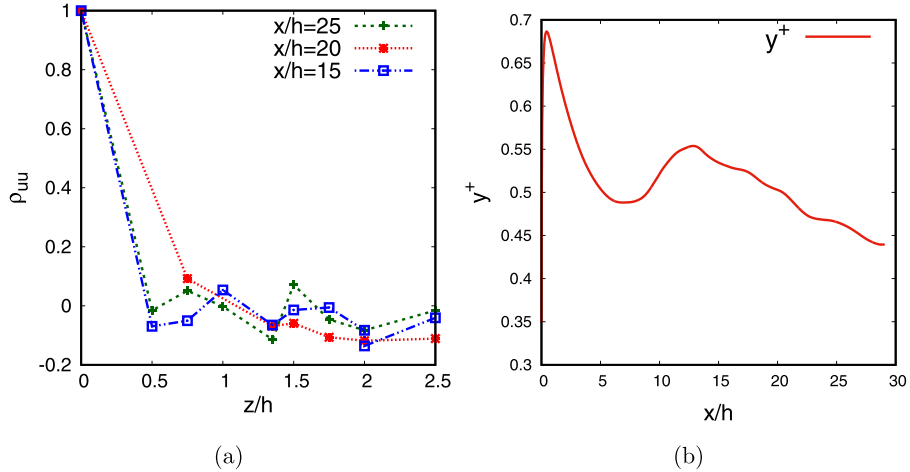


Fig. 2. (a) Span-wise variation of the velocity correlation coefficient at $y/h = 1$. (b) Axial variation of y^+ , the centroid of the first-cell away from the wall.

within the simulation domain. The wall above the inlet boundary is treated as adiabatic, and the bottom wall is treated as an isothermal wall with a temperature of 350 K which is higher than the ambient temperature of 298.15 K. The temperature of the incoming jet flow is set the same as the ambient temperature. A turbulent wall-jet is nearly self-similar in the region beyond $x/h = 20$ [6,12] therefore, the domain is restricted to $30h$ in the stream-wise direction (axial) due to limited computational resources. The domain is extended by $10h$ in the wall-normal direction, and $5.5h$ in the span-wise direction. To obtain homogeneity in the span-wise direction a periodic boundary condition is applied. The length of the domain used in the present study is found to be sufficient owing to the self-similar profiles being observed beyond $x/h = 20$. In order to check whether the span-wise width used was sufficient or not to obtain homogeneity, the two-point correlation of the velocity fluctuations are computed. As can be seen from Fig. 2a, the correlation coefficient of the velocity fluctuations drops quickly within a distance of $z/h = 1$ to less than 14 percent, indicating ho-

mogeneity in the span-wise direction. All the statistics reported in the present work are collected, after an initial transient of 10 flow-through times, for a period of 20 flow-through time.

The domain is discretized using a structured grid of 4 million cells and the same mesh is used for testing all the models. The mesh used has $360 \times 222 \times 50$ cells in the stream-wise, wall-normal and span-wise directions, respectively. About 100 cells are used to accurately resolve the wall-normal direction in the region $0 \leq y/h \leq 1$. The first-cell-centroid away from the wall is ensured to satisfy the condition $y^+ \leq 1$. The axial variation of y^+ along the bottom wall of the domain is shown in Fig. 2b. The mesh used was structured, orthogonal and non-uniform with stretching near the walls.

2.2. Large-eddy simulation (LES) equations

In the present study, OpenFOAM [25,26] is used to solve for the incompressible Navier-Stokes equations using an implicit pressure

algorithm known as PIMPLE to enable pressure-velocity coupling for unsteady problems. Second-order accurate spatial discretization and second-order accurate Crank-Nicholson scheme is used for the time integration. Only for the simulation that used implicit LES, an upwind scheme is used for the spatial discretization in order to numerically stabilize the flow. The filter width in LES that determines the dissipation in sub-grid modeling is defined as $\bar{\Delta}$ which is equal to the cube-root of the volume of each cell, given by, $(\Delta_x \Delta_y \Delta_z)^{1/3}$ where Δ is the grid size, and the subscript denotes the direction. The filtered incompressible, continuity, Navier-Stokes equations, and the energy equation that govern the present problem are given as follows:

$$\frac{\partial \bar{u}_i}{\partial x_i} = 0, \quad (1)$$

$$\frac{\partial \bar{u}_i}{\partial t} + \frac{\partial}{\partial x_j} (\bar{u}_i \bar{u}_j) = -\frac{\partial((\bar{p}/\rho)\delta_{ij} + \tau_{ij})}{\partial x_j} + \nu \frac{\partial^2 \bar{u}_i}{\partial x_j \partial x_j} \quad (2)$$

where \bar{u}_i is the filtered velocity, \bar{p} is the filtered pressure, t is the time, ν is the kinematic viscosity and $\tau_{ij} = \bar{u}_i \bar{u}_j - \bar{u}_i \bar{u}_j$ is the SGS stress tensor. The SGS stress tensor is modeled using Boussinesq hypothesis and can be expressed as follows:

$$\tau_{ij} = -2\nu_t \bar{S}_{ij} + \frac{1}{3} \tau_{kk} \delta_{ij} \quad (3)$$

where δ_{ij} is the Kronecker delta, and ν_t is the turbulent viscosity, \bar{S}_{ij} is the filtered strain rate tensor given by $\frac{1}{2} \left(\frac{\partial \bar{u}_i}{\partial x_j} + \frac{\partial \bar{u}_j}{\partial x_i} \right)$. The filtered energy equation can be written as follows:

$$\frac{\partial \bar{T}}{\partial t} + \frac{\partial}{\partial x_j} (\bar{T} \bar{u}_j) = \alpha \frac{\partial^2 \bar{T}}{\partial x_j \partial x_j} + \frac{\partial q_j}{\partial x_j} \quad (4)$$

where $q_j = \bar{T} \bar{u}_j - \bar{T} u_j$ is the heat flux modeled similar to eddy-viscosity and this is known as an eddy-diffusivity model. Using this model, the turbulent heat flux can be defined as $\bar{q}_j = \alpha_t \frac{\partial \bar{T}}{\partial x_j}$, where α_t is the eddy diffusivity and is evaluated using turbulent Prandtl number with the relation $\alpha_t = \frac{\nu_t}{Pr_t}$, and the molecular diffusivity is defined as $\alpha = \frac{\nu}{Pr}$. In the present study the Prandtl number Pr is taken as 0.71 for air. The values of ν_t and α_t are calculated based on the SGS model used. In the case of implicit LES simulations, the turbulent dissipation is completely due to the numerical dissipation and there the turbulent eddy viscosity, ν_t , and turbulent eddy diffusivity, α_t are set to zero.

2.3. Details of SGS models

The SGS models used in the present study can be classified into two types, one being the constant-coefficient models such as the Smagorinsky model [27], one-equation model [28], wall-adapting local eddy-viscosity model (WALE) [29] in which the coefficients are defined globally and are constant during the entire simulation, and other being the dynamic models such as the dynamic one-equation model [30] and the dynamic Smagorinsky model [31] where the coefficients are calculated locally as function of space at each time step. All the SGS models used in the present work is discussed in the following sub-sections.

2.3.1. The constant coefficient Smagorinsky model

In the constant coefficient Smagorinsky model, the turbulent viscosity in the equation (3) is calculated as:

$$\nu_t = (C_s \bar{\Delta}^2) |\bar{S}| \quad (5)$$

where $|\bar{S}|$ is the magnitude of filtered strain rate tensor given by $|\bar{S}| = \sqrt{2\bar{S}_{ij}\bar{S}_{ij}}$, $\bar{\Delta}$ is the filter width, and C_s is the constant of the model which is taken as 0.168 in the present work.

2.3.2. One-equation model for subgrid-scale kinetic energy

In this model the local equilibrium assumption of sub-grid scale production and dissipation like in the Smagorinsky model is not made and the K_{sgs} is directly implemented in the equation 3 written as

$$\tau_{ij} = -2\nu_t \bar{S}_{ij} + \frac{2}{3} k_{sgs} \delta_{ij} \quad (6)$$

and the turbulent viscosity ν_t can be expressed as,

$$\nu_t = (C_k \bar{\Delta}) k_{sgs}^{1/2} \quad (7)$$

where the SGS kinetic energy k_{sgs} is defined as,

$$k_{sgs} = \frac{1}{2} \left(\bar{u}_i^2 - \bar{u}_i^2 \right) \quad (8)$$

which is obtained by solving the following transport equation,

$$\frac{\partial k_{sgs}}{\partial t} + \frac{\partial \bar{u}_i k_{sgs}}{\partial x_j} = -\tau_{ij} \frac{\partial \bar{u}_i}{\partial x_j} - \frac{C_e k^{1.5}}{\bar{\Delta}} + \frac{\partial}{\partial x_j} \left(\nu_t \frac{\partial k_{sgs}}{\partial x_j} \right) \quad (9)$$

where the coefficients C_e and C_k are taken to be $C_e = 1.048$ and $C_k = 0.094$.

2.3.3. Wall-adapting local eddy-viscosity (WALE) model

The WALE model was developed in order to correctly model the asymptotic behavior of turbulent eddy-viscosity near the walls, which was a shortcoming in the constant coefficient eddy-viscosity models. In this model the value of ν_t is obtained as,

$$\nu_t = (C_w \bar{\Delta}^2) \frac{(S_{ij}^d S_{ij}^d)^{\frac{3}{2}}}{(\bar{S}_{ij} \bar{S}_{ij})^{\frac{5}{2}} + (S_{ij}^d S_{ij}^d)^{\frac{5}{4}}} \quad (10)$$

where S_{ij}^d is the traceless part of the square of the velocity gradient tensor, given by,

$$S_{ij}^d = \frac{1}{2} \left[\left(\frac{\partial \bar{u}_k}{\partial x_i} \frac{\partial \bar{u}_j}{\partial x_k} \right) + \left(\frac{\partial \bar{u}_k}{\partial x_j} \frac{\partial \bar{u}_i}{\partial x_k} \right) \right] - \frac{1}{3} \delta_{ij} \left(\frac{\partial \bar{u}_k}{\partial x_k} \frac{\partial \bar{u}_k}{\partial x_k} \right), \quad (11)$$

where the coefficient of the WALE model C_w is taken to be 0.325.

2.3.4. Dynamic Smagorinsky model

In the dynamic models, the model coefficients are no more constant and they are evaluated locally, based on the flow field information using a test filter. Generally, the test filter, denoted with a hat, $\hat{\Delta}$, is taken to be twice as large as the grid filter, that is $\hat{\Delta} = 2\bar{\Delta}$. Eq. (2) is further filtered using this test-filter and the resulting equation can be written as,

$$\frac{\partial \hat{u}_i}{\partial t} + \frac{\partial}{\partial x_j} (\hat{u}_j \hat{u}_i) = -\frac{\partial((\hat{p}/\rho)\delta_{ij} + \hat{\tau}_{ij})}{\partial x_j} + \nu \frac{\partial^2 \hat{u}_i}{\partial x_j \partial x_j} \quad (12)$$

where the constant coefficient in Eq. (5) is calculated with the test-filter using the method of least-squares as proposed by Germano [31] and later modified by Lilly [32] and can be written as,

$$C_s^2 = -\frac{\langle L_{ij} M_{ij} \rangle}{2 \langle M_{ij} M_{ij} \rangle} \quad (13)$$

where the L_{ij} stress terms that arise due to the test-filter contain the resolved scales between the grid-filter and the test-filter and are given by,

$$L_{ij} = \widehat{\bar{u}_i} \widehat{\bar{u}_j} - \widehat{\bar{u}_i} \widehat{\bar{u}_j} \quad (14)$$

and the M_{ij} stress terms are given by,

$$M_{ij} = -\left(\hat{\Delta}^2 |\hat{S}| \hat{S}_{ij} - \hat{\Delta}^2 |\hat{S}| \hat{S}_{ij} \right) \quad (15)$$

To provide stability, the dynamically obtained coefficient C_s is locally weighted averaged and is allowed to take positive values only.

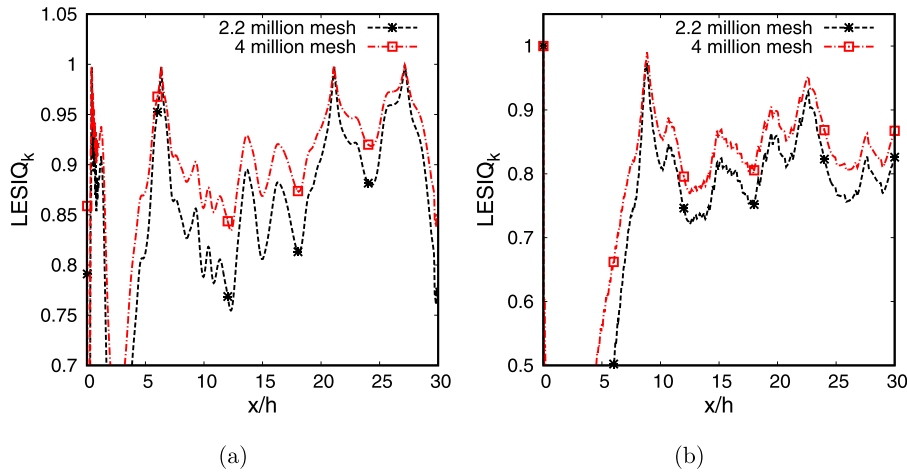


Fig. 3. Axial variation of LESIQ metric for (a) the dynamic one-equation model (b) the Smagorinsky model.

2.3.5. Dynamic one-equation model

In the dynamic one-equation for k_{sgs} model, the evolution equation for k_{sgs} , given by Eq. (9), is test-filtered and can be written as follows,

$$\frac{\partial k_{sgs}}{\partial t} + \frac{\partial \widehat{u}_j k_{sgs}}{\partial x_j} = -\tau_{ij} \frac{\partial \widehat{u}_i}{\partial x_j} - \frac{C_e k^{1.5}}{\widehat{\Delta}} + \frac{\partial}{\partial x_j} \left(v_t \frac{\partial k_{sgs}}{\partial x_j} \right). \quad (16)$$

To calculate the model coefficient C_k in Eq. (9) and C_e in the above equation, a scale-similarity assumption along with the least-square method is used to locally calculate the coefficients. C_k is computed as:

$$C_k = \frac{1}{2} \frac{t_{ij}\sigma_{ij}}{\sigma_{ij}\sigma_{ij}} \quad (17)$$

where, $t_{ij} = \widehat{\bar{u}_i \bar{u}_j} - \widehat{\bar{u}_i} \widehat{\bar{u}_j}$ and $\sigma_{ij} = \widehat{\Delta} \left(\frac{1}{2} (\widehat{\bar{u}_i \bar{u}_i} - \widehat{\bar{u}_i} \widehat{\bar{u}_i}) \right)^{\frac{1}{2}} \widehat{\bar{S}_{ij}}$. The coefficient C_e is solved using equation:

$$C_e = \frac{\nu \left(\left(\widehat{\frac{\partial \tilde{u}_i}{\partial x_j} \frac{\partial \tilde{u}_i}{\partial x_j}} \right) - \widehat{\frac{\partial \tilde{u}_i}{\partial x_j}} \widehat{\frac{\partial \tilde{u}_i}{\partial x_j}} \right)}{\frac{1}{2} \left(\widehat{\tilde{u}_i} \widehat{\tilde{u}_i} - \widehat{\tilde{u}_i} \widehat{\tilde{u}_i} \right)^{\frac{3}{2}}} \quad (18)$$

The coefficient are stable as the denominator is made of resolved energy term which is non-zero.

2.3.6. Eddy-diffusivity model

In this section, the modeling used for the turbulent Prandtl number, Pr_t is discussed. The value of Pr_t is required, in Eq. (4) for calculating the value of eddy-diffusivity, α_t . In the constant coefficient models, the Pr_t value is taken to be constant and equal to 0.85 [33]. In the dynamic models, the Pr_t is allowed to vary within the domain. The algorithm to calculate Pr_t is the same as described by Germano and later modified by Lilly [32]. This algorithm is implemented in OpenFOAM and tested to study the effect of variable Pr_t on the solution. At each grid point the value of Pr_t is calculated as $Pr_t = C_s^2/C_{Pr_t}^2$, where C_{Pr_t} is obtained using the method of least-squares as, $C_{Pr_t}^2 = \frac{\langle P_j R_j \rangle}{2\langle R_j \hat{R}_j \rangle}$. The temperature flux terms related to the test-filter, P_j are given by, $P_j = \widehat{u_j T} - \widehat{\bar{u}_j \bar{T}}$ and the R_j temperature fluxes are given by, $R_j = \widehat{\Delta^2 |\hat{S}|} \frac{\partial \hat{T}}{\partial x_j} - \widehat{\Delta^2 |\bar{S}|} \frac{\partial \bar{T}}{\partial x_j}$. The computed values of Pr_t are allowed to take values in the range of 0.5 to 1.2 and the values falling outside this range are clipped to the minimum or maximum values specified.

2.4. Grid resolution study

The adequacy of the grid resolution used in the present study for the performing LES is verified using the LES index of resolution quality (LESIQ) proposed by Celik et al. [34]. Two cases with grid resolutions of 2.2 million cells and 4 million cells are used to obtain the constant $LESIQ_k$ – the ratio of resolved to the total turbulent kinetic energy.

The total kinetic energy is obtained by using Richardson extrapolation of the two turbulent kinetic energies calculated using the two cases with different grid resolutions. The LESIQ_k for the dynamic model and the Smagorinsky model are shown in Fig. 3a and b respectively. The LESIQ values more than 0.8 is considered to be a well-resolved grid for LES [34]. In Fig. 3a for the dynamic one-equation model it is observed that the grid is well-resolved with LESIQ higher than 0.8 in the turbulent region, which is the area of interest, but the coarser 2.2 million grid is under-resolved. This under-resolution can be noticed in the grid-sensitivity plot for tke, as shown in Fig. 4aa, and the stream-wise Reynolds stress plot, as shown in Fig. 4b. It can be seen from Fig. 4b that the dip in the profile of the inner layer for a mesh of 4 million cells tends towards the experimental data of Eriksson et al. [6]. There is no variation in the stream-wise mean velocity as can be seen from Fig. 4c.

Further, in order to check whether the existing grid, with 4 million cells, resolves the turbulence energy cascade process in the inertial range or not, the energy spectrum is computed and shown in Fig. 5. The non-dimensional frequency is calculated as $S = \frac{hf}{U_0}$. From this figure, we can observe a well-resolved energy cascade process over a wide range of scales in the inertial range.

3. Results and discussion

In this section, the results obtained are thoroughly discussed. The effect of the variable Pr_t on the solution and the effect of the near-wall Van-Driest damping are reviewed. Further, the activity parameter is used to compare the different models used in terms of their capability to actively model the turbulent dissipation. The variation of mean and second-order statistics are discussed both for the flow and temperature. Finally, the downstream evolution of the Nusselt number is compared between the different models and with the experimental data.

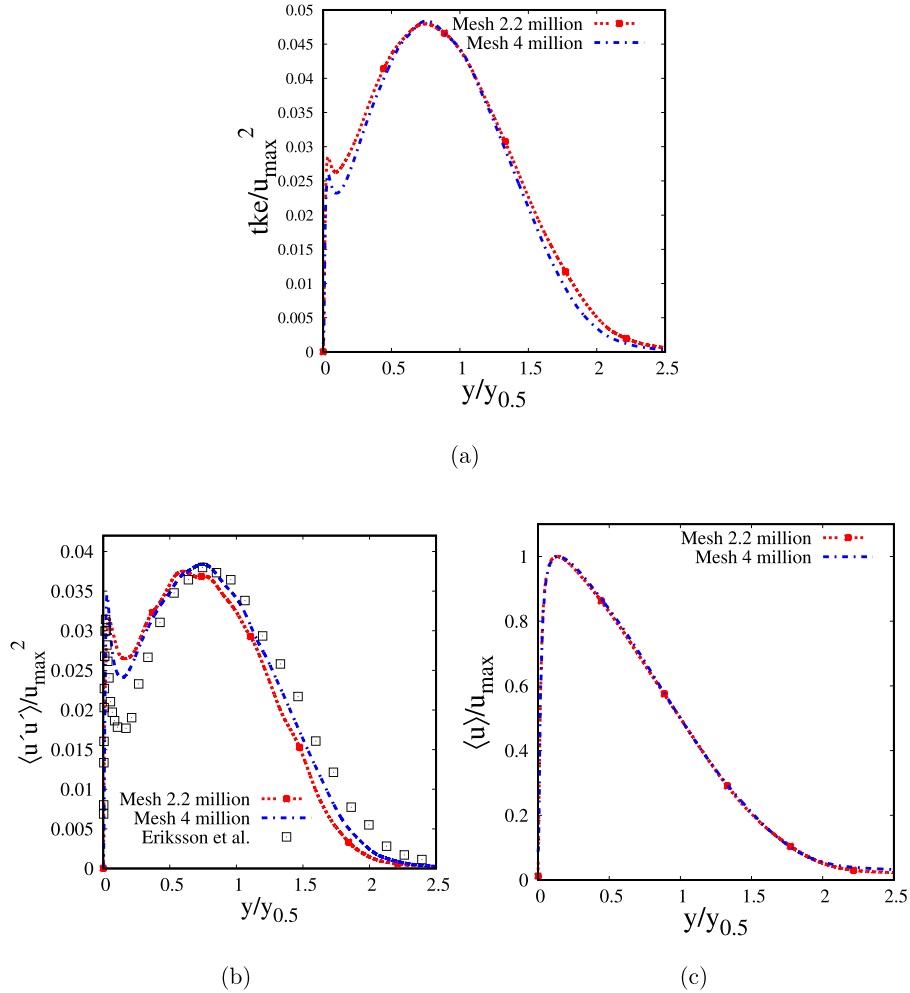


Fig. 4. Variation due to grid-resolution in the (a) the turbulent kinetic energy (b) mean stream-wise Reynolds stress (c) mean stream-wise velocity.

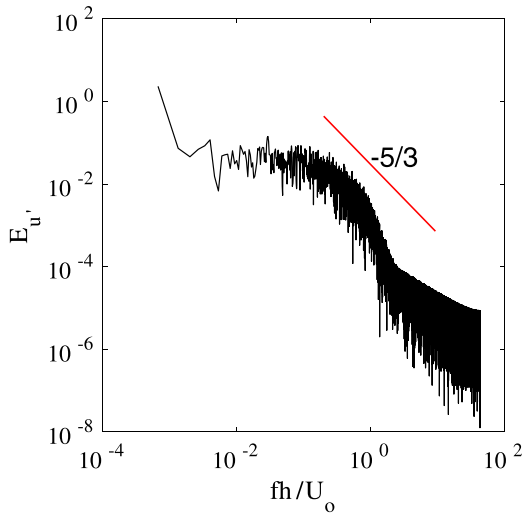


Fig. 5. The energy spectrum at the location of $x/h = 25$ and $y/h = 1$.

3.1. Effect of variable turbulent Prandtl number

The effect of variable Pr_t on the solution is studied in this section. The results obtained using the variable Pr_t implementation are compared with that of the constant $Pr_t = 0.85$. In the variable

Pr_t implementation the computed value of the Pr_t is clipped so as to lie between 0.5 and 1.20. These limits were chosen from the variation obtained in the DNS simulations from the literature [16]. The instantaneous variation of Pr_t with the wall-normal direction is shown in Fig. 6 at $x/h = 25$. From this figure, it can be noted that Pr_t values vary as one moves away from the wall.

The variation of mean temperature and rms temperature in the wall-normal direction are shown in Fig. 7a and b respectively for the constant Pr_t and for the variable Pr_t cases. From the variation of mean temperature it can be noted that the use of variable Pr_t has a negligible effect on the solution. Further, the location and magnitude of the peak of the T_{rms} remained the same between the two implementations. However, there seem to be some small differences as one moves away from the wall, and the variable Pr_t shows higher T_{rms} values when compared with the constant Pr_t implementation.

3.2. Effect of Van-Driest damping

One of the shortcomings of the constant coefficient Smagorinsky model is that the turbulent viscosity, ν_t , does not decay to zero as one approaches the wall. In order to address this problem, near wall Van-Driest damping function was used. This damping function modifies the definition of the local filter-width, Δ , which further properly damps the turbulent viscosity. The definition of Δ is modified by choosing a minimum of, $\frac{\kappa y}{C_s} D$ and Δ where the value

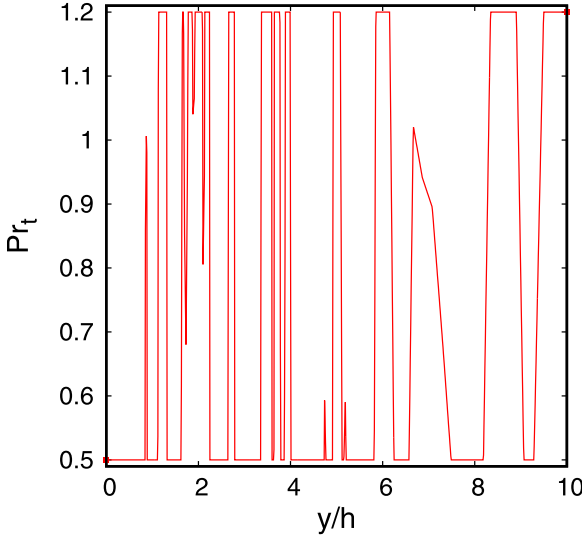


Fig. 6. Variation of turbulent Prandtl number in the wall-normal direction at $x/h = 25$.

of D is calculated as, $D = 1 - \exp\left(-\frac{y^+}{A^+}\right)$. The coefficients used are $A^+ = 26$, $C_s = 0.1$ and $\kappa = 0.41$.

The near-wall decay of the ratio of turbulent viscosity to the molecular viscosity, ν_t/ν along y^+ , is shown in Fig. 8. The theoretical damping of the turbulent viscosity should scale as y^{+3} . From this figure, it is seen that the viscosity ratio, ν_t/ν , obtained using the Smagorinsky model without Van-Driest damping does not decay to zero as one approaches the wall. However, the viscosity ratio obtained using Van-Driest model shows a correct decay towards the wall and matches the theoretical decay rate. The viscosity ratio obtained using the dynamic one-equation model shows a decay towards zero as one approaches the wall with a close match to the theoretical decay rate. In order to further understand the effect of Van-Driest damping, the wall-normal variation of axial velocity is plotted, using inner-scaling, in Fig. 9. From this figure, it can be noted that the results obtained using the Smagorinsky model with Van-Driest damping correctly captures the velocity profile when compared with the experimental data. The results obtained using the Smagorinsky model without Van-Driest model over-predict the velocity variation in peak. The reason for this over-prediction is attributed to the incorrect near-wall behavior of ν_t that is observed in Fig. 8.

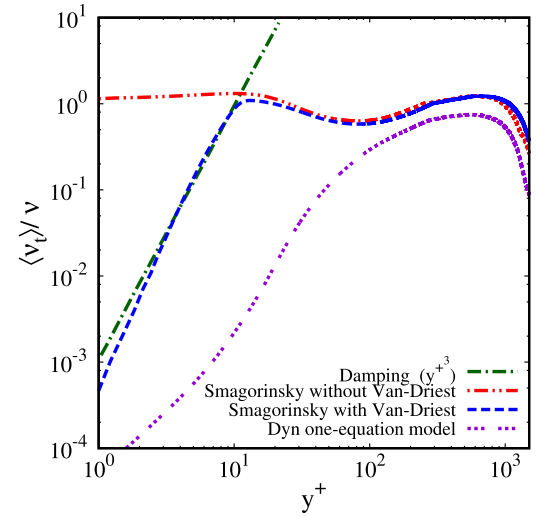


Fig. 8. Near-wall variation of the viscosity ratio, ν_t/ν , for the indicated models

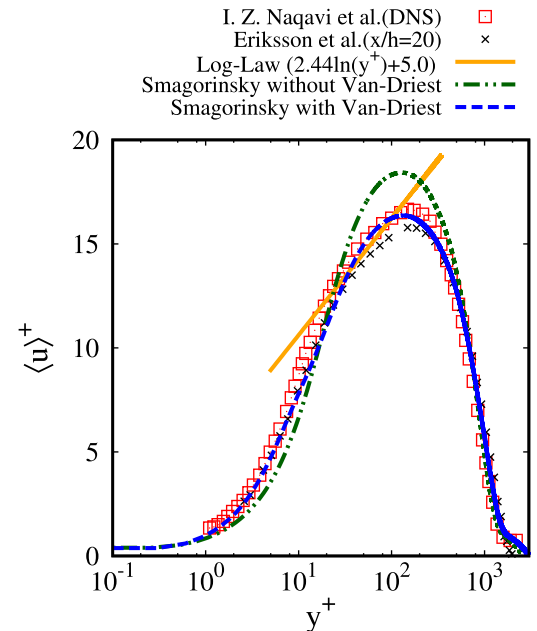


Fig. 9. wall-normal variation of mean axial velocity using inner-scaling at $x/h=25$ for the indicated models.

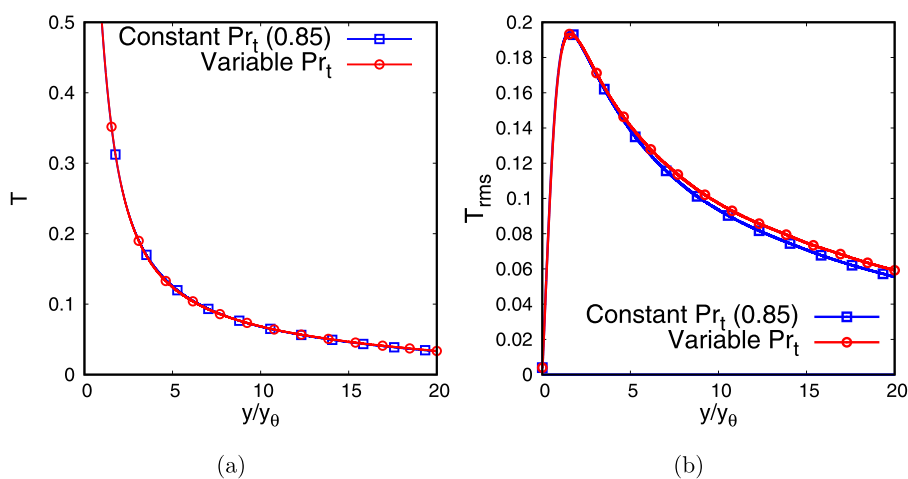


Fig. 7. (a) Wall-normal variation of mean temperature at $x/h = 25$ (b) wall-normal variation of T_{rms} at $x/h = 25$.

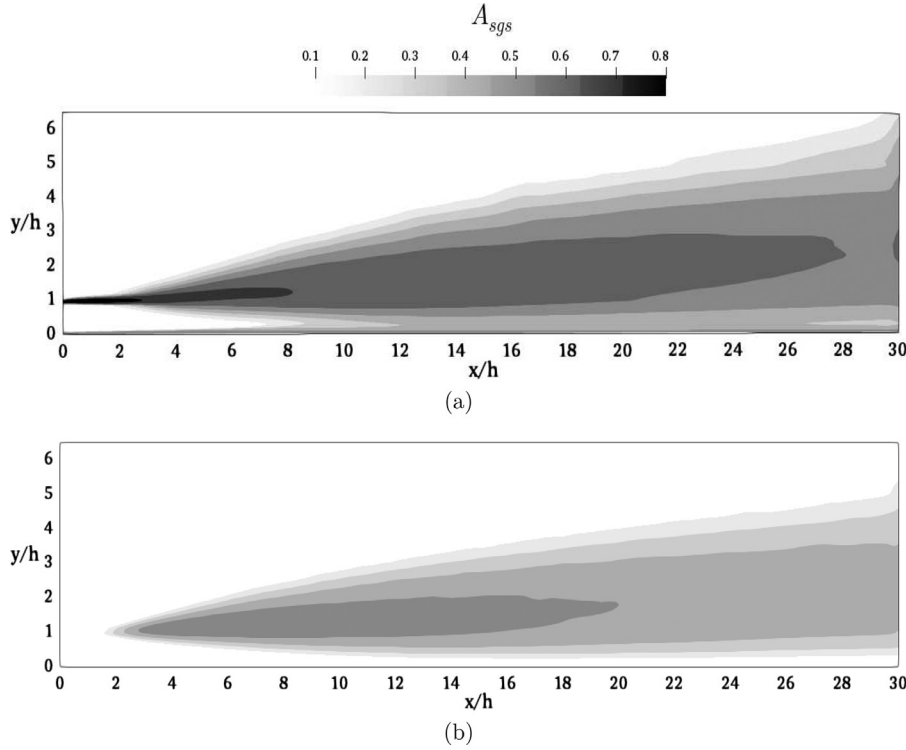


Fig. 10. Velocity Contours of time-averaged SGS activity parameter, $\langle A_{sgs} \rangle$, for (a) the Smagorinsky model (b) the dynamic one-equation model.

3.3. SGS activity parameter

The SGS activity parameter is defined as, $\langle A_{sgs} \rangle = \frac{v_t}{(v_t + v)}$, where the angle-brackets denote a time-averaged value [35]. The amount of dissipation provided by a particular SGS model can be evaluated using this parameter. The values of A_{sgs} vary between 0 and 1, where a value of 0 corresponds to DNS and a value of 1 corresponds to LES for a very large Reynolds number [35]. In the present case, the maximum value of the activity parameter is found to be around 0.8. The contours of $\langle A_{sgs} \rangle$ are shown in Fig. 10a and b for the Smagorinsky and dynamic one-equation model respectively.

From Fig. 10a and b, it is noted that the Smagorinsky model induces more dissipation than the dynamic one-equation model which is expected as the Smagorinsky model would be adding dissipation in all the regions of the flow field. Owing to the Van-Driest damping function used in the Smagorinsky model, the $\langle A_{sgs} \rangle$ parameter is active all the way towards the wall and it gets damped and reaches a value of zero as one approaches the wall. In the dynamic one-equation model, as the SGS viscosity is computed locally the activity parameter decreases gradually as one approaches the wall. The near-wall behavior of the activity parameter for the Smagorinsky and the dynamic one-equation models can be clearly seen to be different. The reason for this behavior stems from the fact that v_t for dynamic one-equation model gets damped for $0 \leq y^+ \leq 100$, whereas it gets damped only in the region of $0 \leq y^+ \leq 10$ for the Smagorinsky model with a steeper gradient as can be seen in Fig. 8.

Further, the Smagorinsky model is observed to be active near the inlet which gives it a different evolution profile in the near-inlet-region as compared to the dynamic one-equation model. The iso-surface of Q -criterion is shown in Fig. 11a and b for the Smagorinsky and the dynamic one-equation models respectively. From these Q iso-surface of the dynamic model, the formation of the roller like structures, the near-wall eddies and their break-up can be observed, which demonstrates the ability of this model

to capture the physics. This eddy break up could result in better performance of the model in terms of the second-order statistics. From Fig. 11a it is observed that the three-dimensionality of the vortical structures as well the number of eddies near the bottom wall are much lesser in comparison to the dynamic one-equation model. The reason for the dearth of the number of smaller eddies, near the inlet region and the bottom-wall, in the Smagorinsky model is ultimately related to the $\langle A_{sgs} \rangle$ parameter being very active in these regions. The highly dissipative nature of the Smagorinsky model in this region is responsible for the suppression of these eddies. The activity parameter is noted to be around 25% higher in magnitude for the Smagorinsky model when compared with the dynamic one-equation model.

3.4. Mean and turbulent quantities of the flow field

In this section, the mean and second-order statistics obtained using several SGS models and implicit LES considered in the present study are compared with the experimental data of Eriksson et al. [6]. The scaling used for the outer-layer can be understood from the schematic in Fig. 12a, whereas for scaling the inner-layer, the friction velocity u_τ is used. The self-similarity of the profile can be obtained in the fully turbulent regime using these different inner and outer scalings as identified by Wygnanski et al. [36]. The wall-normal variation of the stream-wise and wall-normal mean velocities, with outer-scaling, is shown in Figs. 12b and 13a respectively. In these plots, the results obtained from all the five SGS models, and the implicit LES are compared with the data from the literature. As seen from these figures, implicit LES fails to capture the variation of mean u/u_{max} and v/u_{max} along the wall-normal direction. All the SGS models accurately predict the variation of $\langle u \rangle/u_{max}$ as can be seen from Fig. 12b. However, in capturing the variation of $\langle v \rangle/u_{max}$, the constant Smagorinsky and constant coefficient one-equation models performed better in the near-wall region, while the dynamic Smagorinsky, dynamic one-

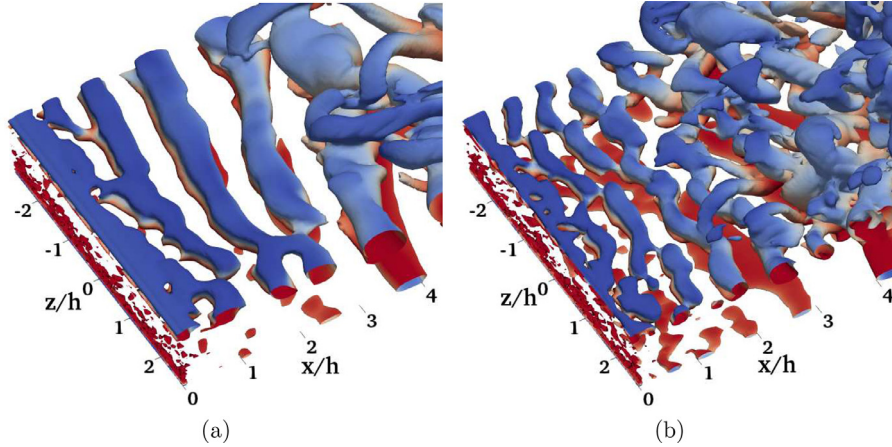


Fig. 11. Iso-surface of the Q-criterion coloured by instantaneous axial velocity near the inlet for (a) the Smagorinsky model (b) the dynamic one-equation model.

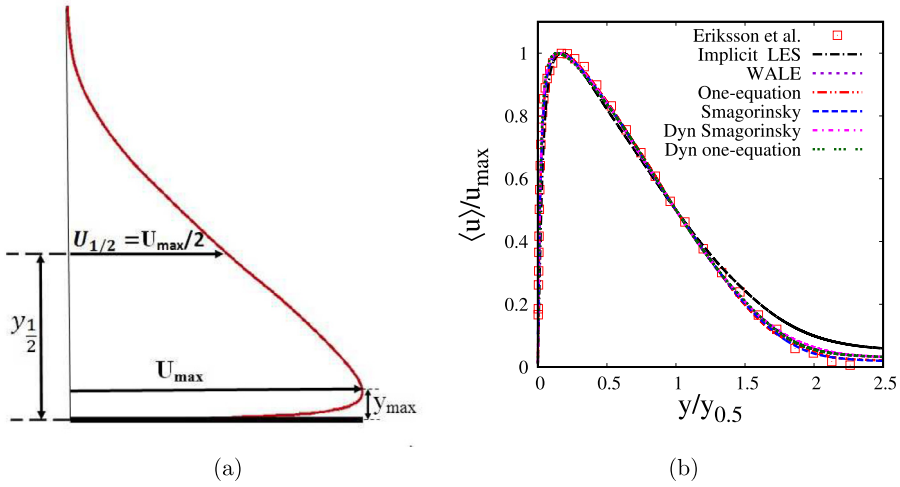


Fig. 12. a) Schematic depicting the outer-scaling (b) Wall-normal variation of the mean stream-wise velocity, at $x/h = 20$.

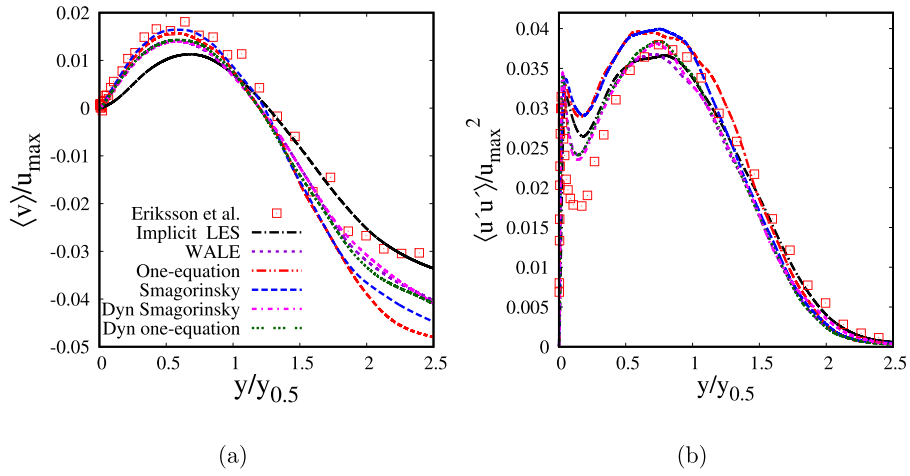


Fig. 13. Wall-normal variation of normalized (a) mean wall-normal velocity (b) Reynolds stress $\langle u' u' \rangle$ when outer-scaled.

equation model and the WALE model predicts well away from the wall.

Next, the variation of the second-order statistics are studied. The wall-normal variation of normalized $\langle u' u' \rangle$ and $\langle v' v' \rangle$ are shown in Figs. 13b and 14a respectively. Fig. 13b shows that, the outer-peak is accurately predicted by the dynamic Smagorinsky and the dynamic one-equation models, however, all the other

models fail to capture the minima seen near the wall. It was noted that the near-wall minima was not captured by the DNS data as well [17]. For the variation of normalized $\langle v' v' \rangle$, the WALE and the dynamic models predict values closer to the experimental data when compared with the constant coefficient models.

The wall-normal variation of normalized Reynolds shear stress, at $x/h = 20$ is shown in Fig. 14b. From this figure, it can be noted

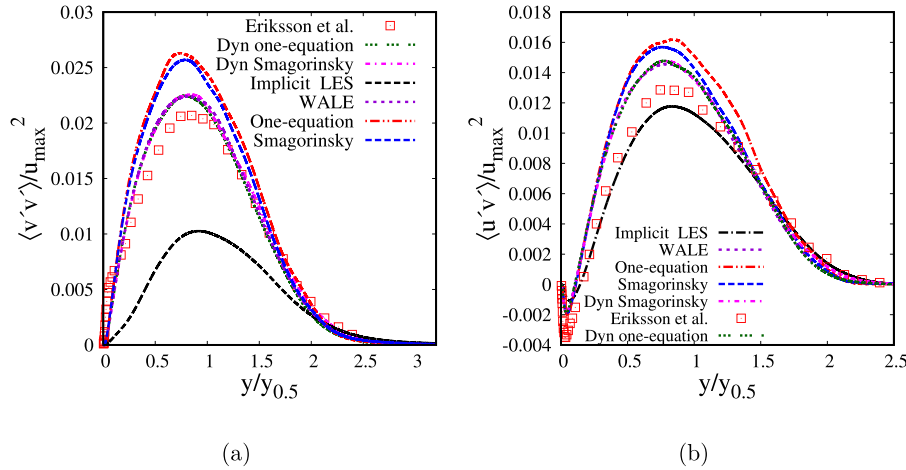


Fig. 14. Wall-normal variation of (a) Reynolds stress $\langle v'v' \rangle$ (b) Reynolds shear stress $\langle u'v' \rangle$ with outer-scaling at $x/h=20$

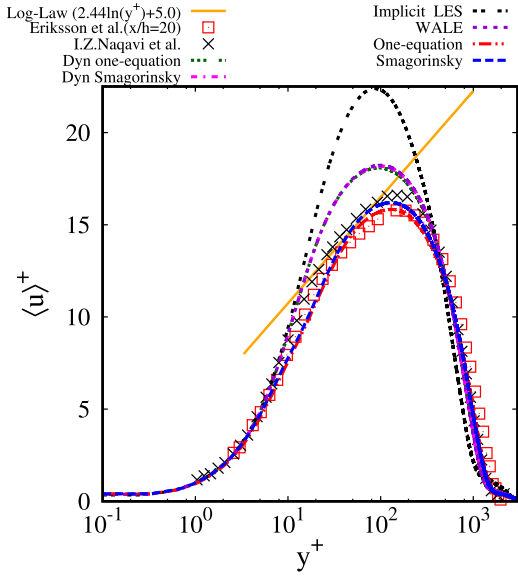


Fig. 15. Variation of inner-scaled mean stream-wise velocity with the wall-normal direction, for the indicated models, at $x/h = 25$.

that the WALE and the dynamic models predict the values closer to the experimental data. The implicit LES under-predicts the values at all the y locations. The constant coefficient Smagorinsky and the one-equation models over-predict the values compared to both the experimental data as well as the dynamic SGS models. The performance of the models is similar to that observed earlier in the context of variation of $\langle v'v' \rangle$.

Next, we focus on the wall-normal variation of the mean and second-order statistics in using inner-scales to evaluate the performance of the SGS models. The variation of mean stream-wise velocity with the wall-normal direction, with inner-scaling, is shown in Fig. 15 for all the models considered. This figure also includes the DNS data obtained by Naqavi et al. [16] at the location $x/h = 25$. From this figure, it can be observed that the Smagorinsky model and the one-equation model predict the velocity-peak well. These models also accurately follow the theoretical scaling given by the log-law, $2.44\ln(y^+) + 5.0$, over a range of y^+ from 75 to 100. The profiles obtained using these models collapse with the experimental results of Eriksson et al. [6] at the location $x/h = 20$ indicating self-similarity. For the dynamic and WALE models when

used with the inner-scale, there is an over-prediction of the peak as a result of the under-prediction of the friction velocity and thus, the velocity-gradient at the wall. This under-prediction is attributed to the improper damping of the dynamic models near the wall, as was discussed earlier.

Next, the variation of the u_{rms} and v_{rms} in the wall-normal direction is shown in Fig. 16a and b. In both the figures, the implicit LES fails to capture the magnitude as well as the location of the peaks. The dynamic models, as well the WALE model, capture the correct variation of u_{rms} qualitatively. However, the magnitude is over-predicted. The Smagorinsky and the one-equation models have an abrupt change in the variation of u_{rms} in the range of $5 \leq y^+ \leq 10$. This abrupt change is attributed to the sudden change in the slope of the turbulent viscosity that was observed in Fig. 8 around $y^+ = 13$. The constant coefficient models, however, are closer to the experimental data for both u_{rms} and v_{rms} .

3.5. Turbulence energy budgets

In this section, the turbulence energy budgets are evaluated for constant coefficient Smagorinsky model and the dynamic one-equation model. An evaluation of the turbulence budgets will help in understanding how the models perform in capturing the interaction of the inner and outer layers. The equation of Reynolds stress tensor for the budgets using tensor notation is referred from [17] and is given as follows:

$$C_v \langle u'_i u'_j \rangle = P_{\langle u'_i u'_j \rangle} + \epsilon_{\langle u'_i u'_j \rangle} + T_d \langle u'_i u'_j \rangle + \psi_{\langle u'_i u'_j \rangle} + D_{\langle u'_i u'_j \rangle} \quad (19)$$

The current LES is performed on a much coarser grid with dissipation $\epsilon_{\langle u'_i u'_j \rangle}$ being calculated as the residue of the above terms. The major budget quantities of a dynamic model (i.e the dynamic one-equation model) and a constant coefficient model (the Smagorinsky model) are then compared with that of the reference DNS by Naqavi et al. [17] measured at $x/h = 30$. The specific terms occurring in the above equation are calculated using following expressions:

$$C_v \langle u'_i u'_j \rangle = \langle u_k \rangle \frac{\partial \langle u'_i u'_j \rangle}{\partial x_k} \quad \text{Convection} \quad (20)$$

$$P_{\langle u'_i u'_j \rangle} = -\langle u'_j u'_k \rangle \frac{\partial \langle u_i \rangle}{\partial x_k} - \langle u'_i u'_k \rangle \frac{\partial \langle u_j \rangle}{\partial x_k} \quad \text{Production} \quad (21)$$

$$T_d \langle u'_i u'_j \rangle = -\frac{\partial \langle u'_i u'_j u'_k \rangle}{\partial x_k} \quad \text{Turbulent diffusion} \quad (22)$$

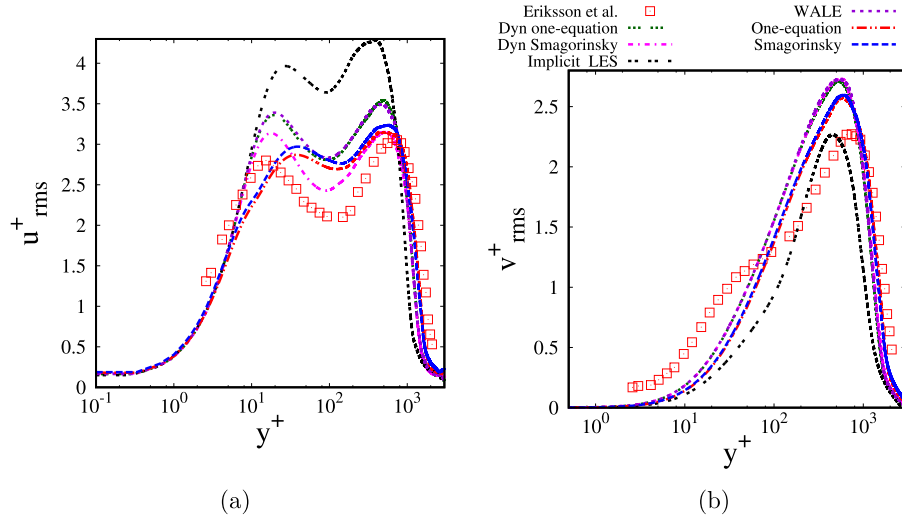


Fig. 16. Wall-normal variation of (a) u_{rms} and (b) v_{rms} with inner-scales.

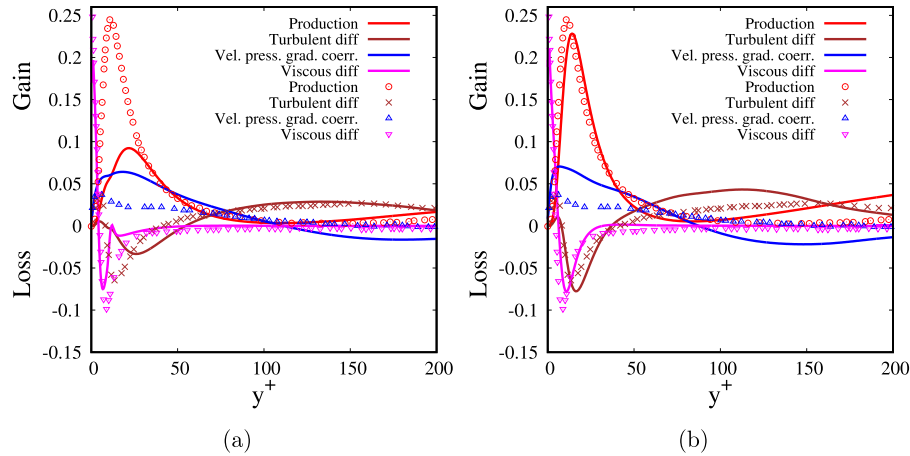


Fig. 17. Inner-scaled turbulent kinetic energy budget (a) Smagorinsky model (b) Dynamic one-equation model

$$\psi_{\langle u'_i u'_j \rangle} = - \left\langle u'_j \frac{\partial p'}{\partial x_i} \right\rangle - \left\langle u'_i \frac{\partial p'}{\partial x_j} \right\rangle \quad (23)$$

Velocity-pressure gradient correlation

$$D_{\langle u'_i u'_j \rangle} = \nu \frac{\partial^2 \langle u'_i u'_j \rangle}{\partial x_k \partial x_k} \quad (24)$$

Viscous diffusion

Fig. 17a and b represent inner-scaled budgets for the turbulent kinetic energy at $x/h = 20$ where, $tke = 0.5 * (\langle u'_i u'_i \rangle + \langle u'_j u'_j \rangle + \langle u'_k u'_k \rangle)$. The Smagorinsky model, as shown in Fig. 17b, under estimates the magnitude of the production term and the turbulent diffusion term near the wall, whereas for the dynamic one-equation model, all the terms in the budgets closely match with that of the DNS as shown in Fig. 17b. Although there is a minor deviation in the peaks away from the wall, the shift in the peak is less than 5 y^+ units. Apart from the velocity-pressure gradient correlation, where dynamic model performs better at $y/y_{1/2} > 0.5$, both the models seem to generate closely matching results for the remaining terms in the budgets equation as shown in Fig. 18a and b.

3.5.1. Velocity-pressure gradient correlation and turbulent transport term

The interaction of the inner and the outer layers of the wall-bounded turbulent jet depends on the turbulent transport, pressure-strain rate, and the pressure diffusion terms [17]. Hence, it is essential to check the capability of the turbulent models to predict these terms accurately. Eq. (23) can be split into a summation of two components, the first component is the pressure diffusion term, calculated as $-\left\langle \frac{\partial}{\partial x_i} \left(p' u'_j \right) + \frac{\partial}{\partial x_j} \left(p' u'_i \right) \right\rangle$ and the second component is the pressure-strain rate term given by $\left\langle p' \left(\frac{\partial u'_j}{\partial x_i} + \frac{\partial u'_i}{\partial x_j} \right) \right\rangle$. The pressure-strain rate term is responsible for the redistribution of the Reynolds stresses in different directions and thus, plays an important role in determining the interaction of layers within the jet. In the present study, the pressure-strain rate and the pressure diffusion term have been calculated explicitly, and the trace of pressure-strain rate in Fig. 19a being zero shows the expected behaviour.

As shown in Fig. 19a, all the models fail to capture the magnitude of pressure diffusion term for turbulent kinetic energy near the wall. In qualitative terms, the dynamic models do have a small change in slope in predicting pressure diffusion term along with a sharp peak for tke as well as $\langle v' v' \rangle$, but the constant-coefficient models could not capture the correct trend. In Fig. 19b, it can

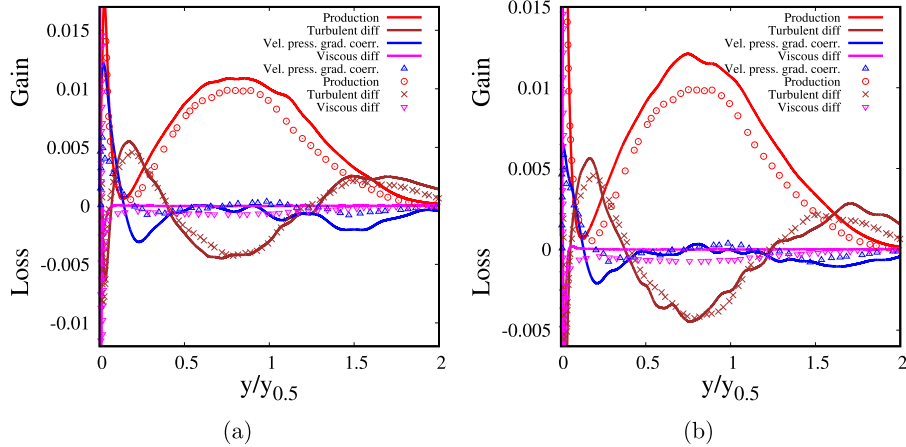


Fig. 18. Outer-scaled turbulent kinetic energy budget (a) Smagorinsky model (b) Dynamic one-equation model

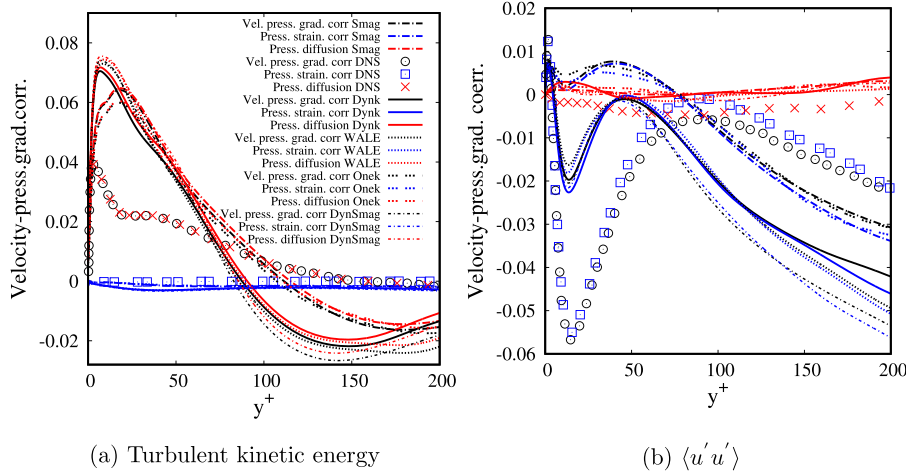


Fig. 19. Inner-scaled velocity pressure gradient correlations at $x/h = 20$ (all the figures have legends as indicated in Fig. 19a).

be seen that all the LES models predict the profiles qualitatively, but the Smagorinsky model and the one-equation model do not change the sign for the pressure-strain correlation in the buffer region. This error in the magnitude prediction leads to lesser redistribution or transfer of energy from the span-wise direction to the stream-wise direction instead of vice-versa. The dynamic models capture this trend qualitatively for the stream-wise Reynolds stress with the a sign change, but they under-predict its magnitude. The wall-normal stress component of the velocity-pressure gradient correlation in Fig. 20a is close to zero for the LES models as the pressure diffusion and the pressure-strain rate terms balance each other. Similar is the case for the velocity-pressure gradient correlation due to the shear-stress, as can be seen in Fig. 20b.

The turbulent transport terms play a significant role in the inner and the outer layer interaction, which is dependent on the gradient of triple velocity correlation as per Eq. (22). Figs. 21a to 22d show the triple correlation profile with the inner and the outer-scaling. From Fig. 21a, it can be noted that, all the models fail to capture the trend, however, the dynamic one-equation model does regain the trend as one moves away from the wall. It can be noticed that apart from the prediction of $\langle u'u'u' \rangle^+$ which has a lesser impact on the budget because of its gradient in the stream-wise direction, the Smagorinsky model and the one-equation model perform well near the wall as compared to the other models. Turbulent transport from outer layer to inner layer is dependent significantly on the gradients of $\langle u'v'v' \rangle$ and $\langle v'v'v' \rangle$ and these param-

ters are negative for $y/y_{0.5} < 0.8$ [17]. All the LES models predict the location of this sign change accurately and thus are able to capture the transfer of shear stress from the outer layer to the inner layer. The dynamic one-equation model predicts the outer-scaled triple velocity correlations relatively better.

3.6. Mean and turbulent quantities of the thermal field

In this section, the mean and second-order statistics obtained using different SGS models are compared with the DNS data. The variation of mean temperature with the wall-normal direction is shown in Fig. 23 for all the models considered together with the DNS data. The Smagorinsky and the one-equation model predict a closer match with the DNS data compared to other models. The reason for the closer match of the temperature profiles is due to the better performance in terms of predicting the velocity profiles near the wall with the aid of damping function. The Implicit LES fails to capture the profiles qualitatively. The wall-normal variation of T_{rms} is shown in Fig. 24. Similar observations as to the variation of mean temperature can be made here. The constant coefficient Smagorinsky and one-equation models are relatively closer to the DNS data. Next, we focus on the variation of turbulent heat flux. The variation of the stream-wise component of turbulent heat flux is shown in Fig. 25a. It can be observed that the one-equation and the constant coefficient Smagorinsky model provide the best results near the peak while all other models agree qualitatively with the DNS data. The wall-normal component of turbulent heat

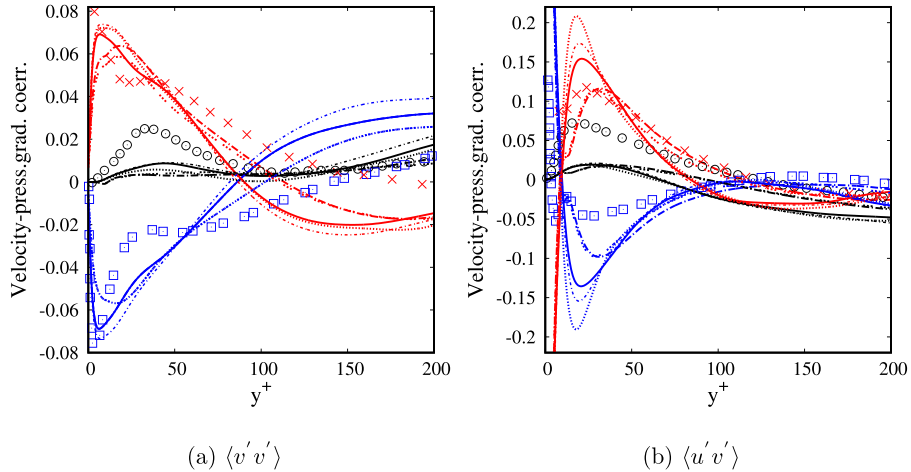


Fig. 20. Inner-scaled velocity pressure gradient correlations (the legends for all the figures are the same as indicated in Fig. 19a).

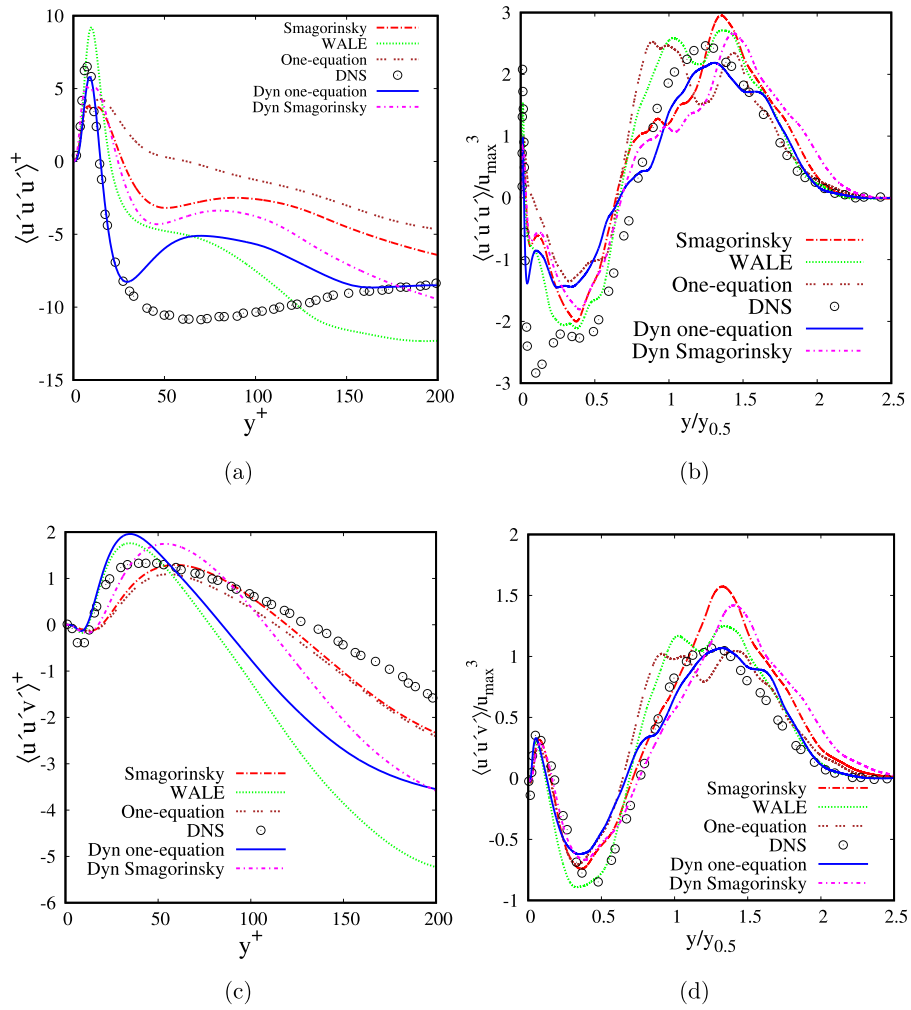


Fig. 21. Inner and outer variation in profiles of triple velocity correlation

flux variation is shown in Fig. 25b. This component of turbulent heat flux is responsible for the transport of heat energy away from the wall. From this figure, it is noted that the constant coefficient Smagorinsky model produces a very close match with the DNS data, whereas the dynamic and the WALE models under-predict the variation. It can also be noted that the one-equation model over-predicts the variation of turbulent heat flux.

Next, we look at the variations of mean and rms temperature and the turbulent heat fluxes with inner-scaling. In order to perform inner-scaling, the temperature parameters are scaled with friction temperature $T_f = \frac{\bar{q}_w}{\rho u_t C_p}$ with, $\bar{q}_w = -k_f \frac{dT}{d\eta} \Big|_{wall}$ where k_f is the thermal conductivity of the fluid, C_p is the specific heat capacity at constant pressure and ρ is the density of the fluid. The vari-

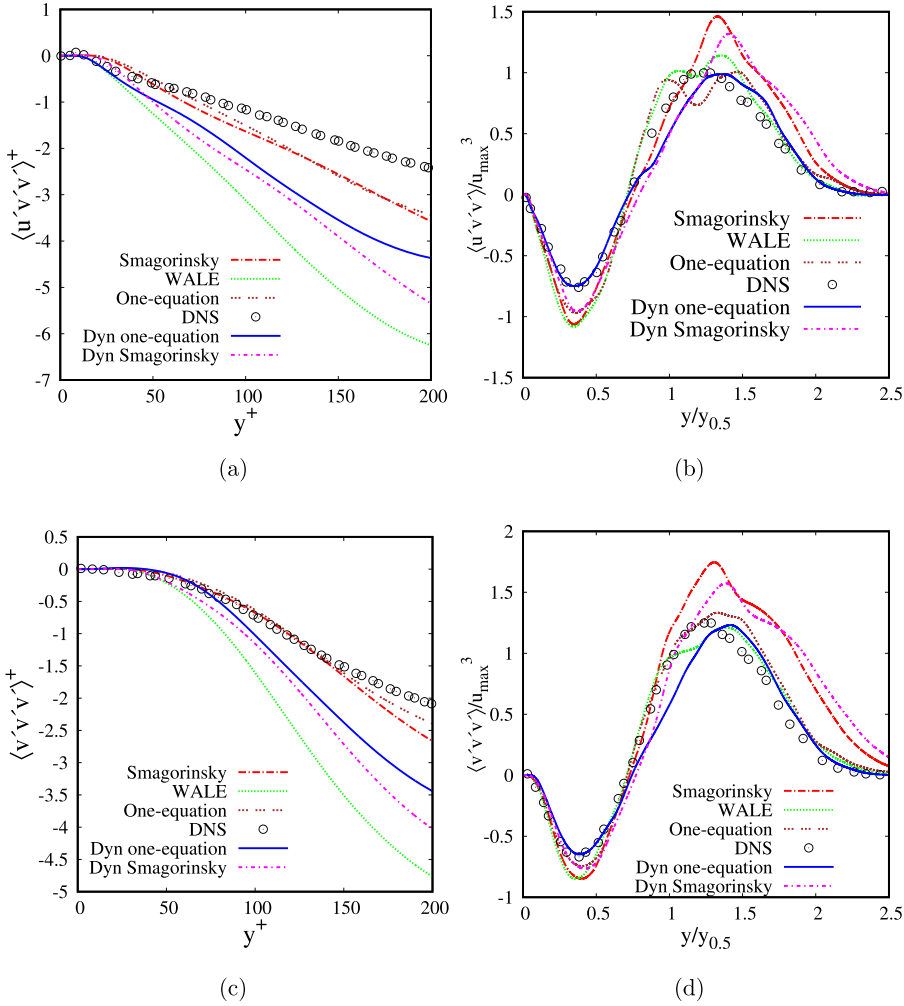


Fig. 22. Inner and outer variation in profiles of triple velocity correlation

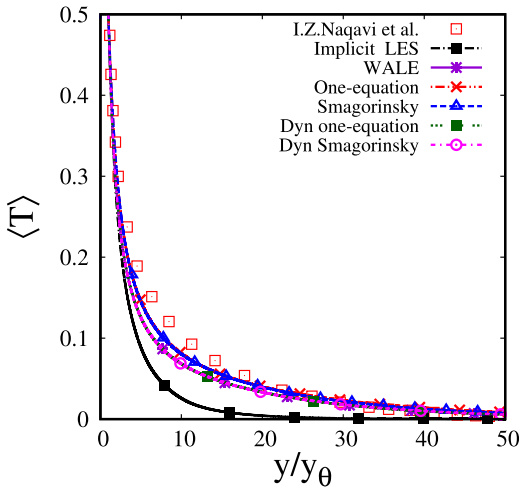


Fig. 23. Variation of outer-scaled mean temperature in the wall-normal direction at $x/h = 25$.

tion of mean temperature with wall-normal direction when inner-scaled is shown in Fig. 26. The inner-scaled mean temperature profiles agree with log-law of $\langle T \rangle^+ = \ln(y^+)/0.48 + 3.5$ for the constant coefficient Smagorinsky and one-equation models over a range of $75 \leq y^+ \leq 105$ with a good match in terms of the mag-

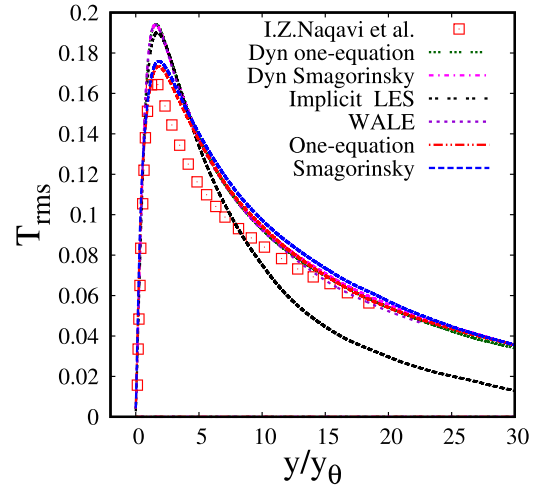


Fig. 24. Variation of outer-scaled rms temperature with the wall-normal direction at $x/h = 25$.

nitude when compared with the DNS data. This is because of the accurate prediction of the friction velocity and friction temperature at the wall by these two models. The variation of T_{rms} in the wall-normal direction is shown in Fig. 27. Similar observations to that

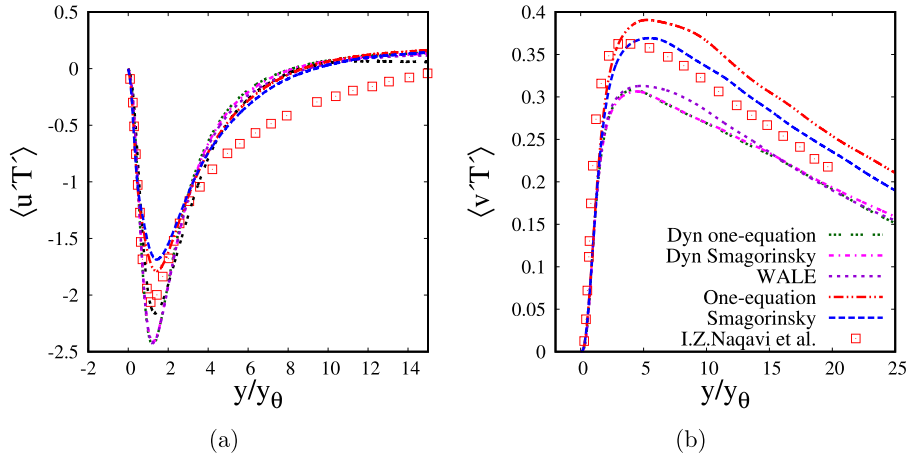


Fig. 25. Wall-normal variation of outer-scaled heat-fluxes (a) $\langle u'T' \rangle$ (b) $\langle v'T' \rangle$. at $x/h=25$.

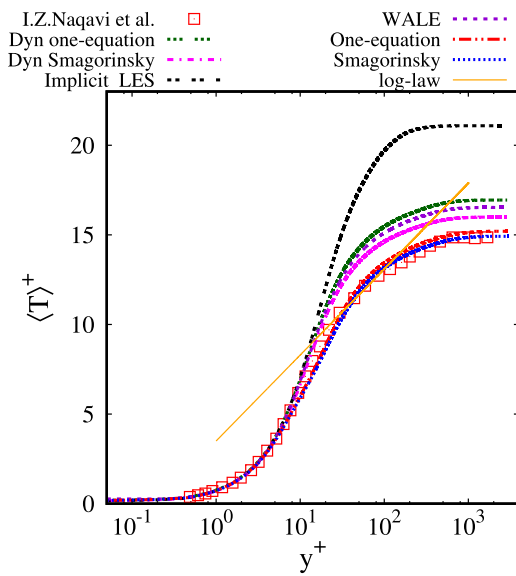


Fig. 26. Variation of inner-scaled mean temperature with y^+ at $x/h = 25$.

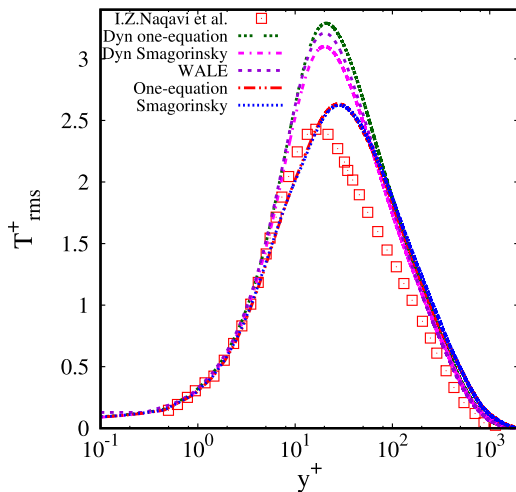


Fig. 27. Variation of T_{rms} with y^+ at location $x/h = 25$ with inner-scales.

made for the variation of mean temperature can be made here. The dynamic and the WALE models over predict the peak for the inner-scaled T_{rms} . The variation of $\langle u'T' \rangle$ with y^+ is shown in Fig. 28a at $x/h = 25$. A negative correlation is observed between the velocity and temperature fluctuations in most of the region. The constant coefficient Smagorinsky and the one-equation model closely capture the negative correlation trough and also under-predict the same when compared to DNS data. An offset can be seen in the location of the trough in comparison to the reference DNS data, and this is attributed to the change in the slope of the v_t curve for these models. A peak is observed away from the wall and has a positive correlation, and the present SGS models predict a higher magnitude than the DNS data. The variation of $\langle v'T' \rangle$ with y^+ is shown in Fig. 28b. All the SGS models predict this variation very closely in terms of magnitude and the location of the peak. The constant coefficient one-equation models gives an exact result when compared with the reference DNS data.

3.7. Axial variation of mean Nusselt number

In this section, the variation of the mean Nusselt number along the downstream direction of the wall is investigated. Further, the flow field is educed using Q-criterion. Fig. 29 shows instantaneous iso-surfaces of Q-criterion, which gives a qualitative description of the flow field produced by the wall-bounded jet. From this figure, rolling structures that are present near the inlet can be observed. Due to Kelvin-Helmholtz instability in the outer shear layer, these vortical structures break down into smaller eddies further downstream. At around $x/h = 6$ the outer-layer interacts with the inner-layer, thus increasing the momentum transfer and the net turbulent heat-flux.

This effect can be observed in the axial variation of mean Nusselt number shown in Fig. 30. From this figure, it can be noted that the heat transfer reduces and attains a minimum near the wall and further downstream it increases to reach a maximum value. This maximum value of the Nusselt number is due to the mixing of the outer cold fluid with the hot fluid in inner-layer. In Fig. 30 the Nusselt number is compared with the experimental data of AbdulNour et al. [8] and the reference DNS data. All the SGS models predict this minimum at $x/h = 6$. The constant coefficient Smagorinsky model and the one-equation model accurately predict the peak of the curve observed in the experiments near the inlet and downstream till $x/h = 13$. The dynamic models does follow the DNS data near the inlet in terms of capturing the minimum. This can be attributed to the SGS models being not active

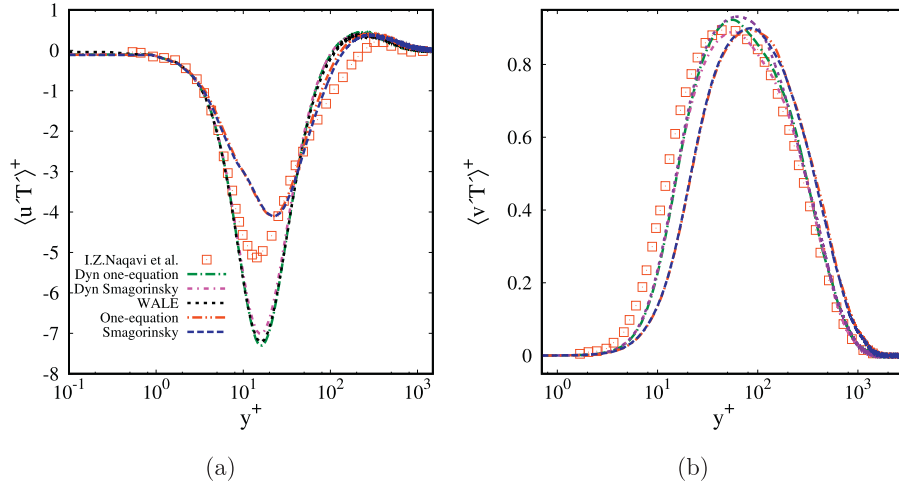


Fig. 28. Variation of inner-scaled heat-fluxes (a) $\langle u' T' \rangle$ with y^+ (b) $\langle v' T' \rangle$ with y^+ at $x/h = 25$.

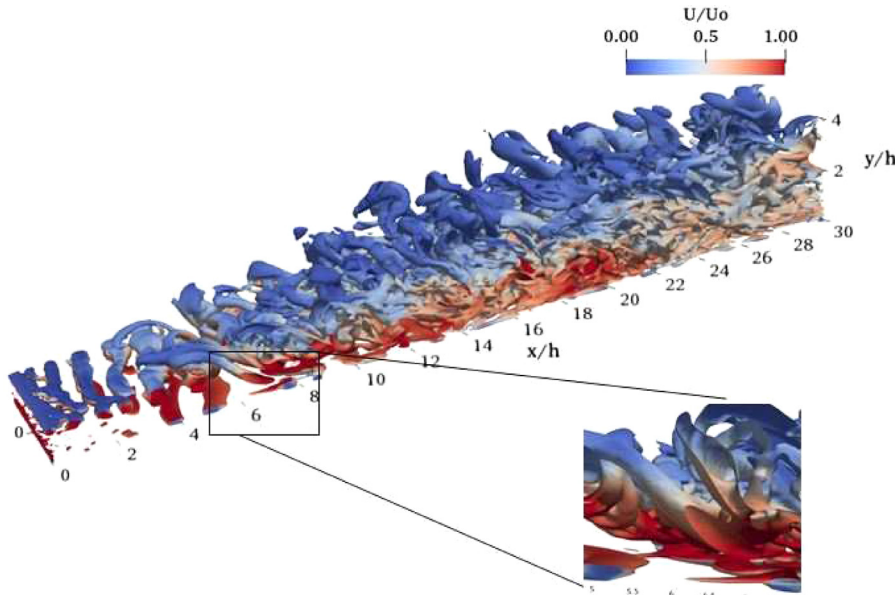


Fig. 29. Iso-surface of the Q-criterion colored by instantaneous axial velocity.

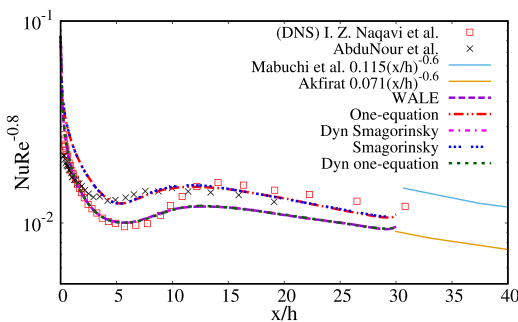


Fig. 30. Stream-wise variation of the mean Nusselt number.

4. Conclusions and future work

In the present work, five different SGS models and implicit LES are evaluated for their performance in simulating planar turbulent wall-bounded jets with heat transfer. The results obtained are compared with the available experimental and the DNS data from the literature. The sufficiency of the mesh resolution used in the present study is evaluated using *LESIQ* metric proposed by Celik et al. [34]. The variation of mean and second-order statistics for the flow and heat transfer, an axial variation of mean Nusselt number, activity parameter, stream-wise and wall-normal components of turbulent heat flux are used in order to evaluate the models. The effect of the Van-Driest damping on the solution is studied. Further, a variable Pr_t algorithm is implemented from the literature, and it is evaluated for the present case. The following conclusions can be drawn from the present work:

- The use of a variable turbulent Prandtl number in the simulations has a negligible effect on the prediction of the thermal characteristics in the near-wall region.

in this region (as shown in Fig. 10b) near the inlet. However, they could not capture the magnitude of the peak. As one moves downstream, all the models fall between the correlation provided by the experiments of Akfirat [4] and Mabuchi and Kumadav [5].

- The implicit LES failed to estimate the velocity and temperature profiles correctly, which justifies the need to use SGS modeling and evaluate their relative predictive capabilities.
 - It is noted that the random isotropic turbulent fluctuations that are superimposed on the mean flow at the inlet are sufficient to induce fluctuations in the wall-jets. Using these random fluctuations, self-similarity in the mean profiles is attained by $x/h = 20$. The results obtained accurately captured both the mean and second-order statistics.
 - The Van-Driest damping function is necessary for the constant coefficient models like the Smagorinsky and the one-equation model. The effect of the damping function on the solution is studied, and it is observed that for these models to correctly capture the flow physics, the damping of ν_t is necessary.
 - The effect of modeling is studied using activity parameter. Excessive damping in the Smagorinsky model leads to less number of resolved eddies as compared to the dynamic one-equation model on the same mesh. This better resolution of the dynamic model is the reason for its superior performance in capturing the Reynolds stresses when compared with the constant coefficient models.
 - It is further observed that even though the Van-Driest damping function when used with Smagorinsky and one-equation models helps in predicting the velocity gradients correctly, and thereby predicts the friction velocity better; it also leads to sudden changes in the turbulent viscosity ν_t and thus affects the inner peak of the stream-wise component of the Reynolds stress and the turbulent heat-flux when used with inner-scaling.
 - All the SGS models considered are able to produce good results for the first-order statistics of velocity. The dynamic models and the WALE model are better at capturing the second-order statistics away from the wall when outer-scaling is used.
 - The constant coefficient Smagorinsky and the one-equation models performed better in capturing the thermal statistics, which are dominant near the wall.
 - The dynamic one-equation model captures the inner-scaled turbulent kinetic energy budget parameters reasonably well. In the outer layer both the constant-coefficient model and the dynamic model are able to predict the correct trend of the turbulent kinetic energy budgets.
 - The transport of turbulent kinetic energy from the outer layer to the inner layer due to triple velocity correlation of $\langle v'v'v' \rangle$ and $\langle u'v'v' \rangle$ is predicted well by the LES models especially the dynamic one-equation model. However, the pressure-strain correlation is under-predicted by LES models and thus, they do not sufficiently redistribute the transported wall-normal energy in the span-wise direction when compared with the DNS. In fact, due to incorrect magnitude predicted for the pressure-strain correlation by the Smagorinsky and the one-equation models, there is an absorption of energy in the buffer region by the stream-wise Reynolds stresses.
 - The ability of subgrid scale LES models can be improved if they can be tuned to capture the magnitude of pressure strain correlation for all the Reynolds stress components correctly.
 - The thermal parameters, including the turbulent heat-fluxes, are captured qualitatively well by all the models and quantitatively well by the constant coefficient Smagorinsky model. Thus LES is an excellent tool to use for the prediction of heat transfer characteristics with a mesh resolution that is smaller by orders of magnitude as compared to the DNS.
 - The reason for the trough observed in the axial variation of mean Nusselt number near the inlet and then its characteristics further downstream are explained with the help of the iso-surface of Q and the interaction of the inner and outer shear layers.
 - The constant coefficient Smagorinsky and the one-equation model performed superiorly better when compared with the experimental data near the inlet for the variation of mean Nusselt number in stream-wise direction. All the SGS models, however, predicted the variation of mean Nusselt number reasonably well further downstream.
- In conclusion, the present work assessed five SGS models and an implicit LES for the simulation of the turbulent wall-bounded jet with heat transfer. The accurate prediction of the wall skin friction coefficient is crucial in order to capture the mean and second-order statistics correctly. The present work can be extended to study the presence of heated obstructions in the flow path of the wall-bounded jet in order to understand the heat dissipation mechanisms. Further, a three-dimensional turbulent jet could also be simulated in order to understand and characterize the flow physics.

CRediT authorship contribution statement

Priyesh Kakka: Software, Validation, Formal analysis, Investigation, Writing - original draft. **Kameswararao Anupindi:** Conceptualization, Methodology, Formal analysis, Supervision, Writing - review & editing.

Acknowledgements

The authors are grateful for the computational resources provided by P.G. Senapathy Center for Computer Resources on the VIRGO computing cluster at Indian Institute of Technology (IIT) Madras. The second author would like to acknowledge the funding received through the new-faculty initiation-grant, MEE1617852NFIGKAME, given by IIT Madras. The comments and suggestions of the anonymous reviewers that helped improve the quality of the manuscript are much appreciated.

References

- [1] B. Launder, W. Rodi, The turbulent wall jet, *Progr. Aerospace Sci.* 19 (C) (1979) 81–128.
- [2] B. Launder, W. Rodi, The turbulent wall jet measurements and modeling, *Ann. Rev. Fluid Mech.* 15 (1) (1983) 429–459.
- [3] A. Sigalla, Measurements of skin friction in a plane turbulent wall jet, *Aeronaut. J.* 62 (576) (1958) 873–877.
- [4] J.C. Akfrat, Transfer of heat from an isothermal flat plate to a two-dimensional wall jet, in: International Heat Transfer Conference Digital Library, Begel House Inc., 1996.
- [5] I. Mabuchi, M. Kumadav, Studies on heat transfer to turbulent jets with adjacent boundaries: 1st report, flow development and mass transfer in plane turbulent wall jet, *Bull. JSME* 15 (88) (1972) 1236–1245.
- [6] J. Eriksson, R. Karlsson, J. Persson, An experimental study of a two-dimensional plane turbulent wall jet, *Exp. Fluids* 25 (1) (1998) 50–60.
- [7] N. Rostamy, D. Bergstrom, D. Sumner, J. Bugg, An experimental study of a turbulent wall jet on smooth and transitionally rough surfaces, *J. Fluid. Eng.* 133 (11) (2011) 111207.
- [8] R. AbdulNour, K. Willenborg, J. McGrath, J. Foss, B. AbdulNour, Measurements of the convection heat transfer coefficient for a planar wall jet: uniform temperature and uniform heat flux boundary conditions, *Exp. Therm. Fluid Sci.* 22 (3-4) (2000) 123–131.
- [9] T. Mondal, M.K. Das, A. Guha, Numerical investigation of steady and periodically unsteady flow for various separation distances between a wall jet and an offset jet, *J. Fluid. Struct.* 50 (2014) 528–546.
- [10] J. Kechiche, H. Mhiri, G. Le Palec, P. Bournot, Application of low Reynolds number $k-\epsilon$ turbulence models to the study of turbulent wall jets, *Int. J. Therm. Sci.* 43 (2) (2004) 201–211.
- [11] S.K. Rathore, M.K. Das, A comparative study of heat transfer characteristics of wall-bounded jets using different turbulence models, *Int. J. Therm. Sci.* 89 (2015) 337–356.
- [12] A. Dejoan, M.A. Leschziner, Large eddy simulation of a plane turbulent wall jet, *Phys. Fluid.* 17 (2) (2005) 025102, doi:10.1063/1.1833413.
- [13] R. Banyassady, U. Piomelli, Turbulent plane wall jets over smooth and rough surfaces, *J. Turbul.* 15 (3) (2014) 186–207.
- [14] R. Banyassady, U. Piomelli, Interaction of inner and outer layers in plane and radial wall jets, *J. Turbul.* 16 (5) (2015) 460–483.
- [15] I.Z. Naqavi, P.G. Tucker, Y. Liu, Large-eddy simulation of the interaction of wall jets with external stream, *Int. J. Heat Fluid Flow* 50 (2014) 431–444.

- [16] I.Z. Naqavi, J.C. Tyacke, P.G. Tucker, A numerical study of a plane wall jet with heat transfer, *Int. J. Heat Fluid Flow* 63 (2017) 99–107.
- [17] I.Z. Naqavi, J.C. Tyacke, P.G. Tucker, Direct numerical simulation of a wall jet: flow physics, *J. Fluid Mech.* 852 (2018) 507–542.
- [18] C. He, Y. Liu, Large-eddy simulation of jet impingement heat transfer using a lobed nozzle, *Int. J. Heat Mass Transf.* 125 (2018) 828–844.
- [19] Z.-w. Li, W.-x. Huai, J. Han, Large eddy simulation of the interaction between wall jet and offset jet, *J. Hydrodyn.* 23 (5) (2011) 544–553.
- [20] N.S. Ghaisas, D.A. Shetty, S.H. Frankel, Large eddy simulation of thermal driven cavity: Evaluation of sub-grid scale models and flow physics, *Int. J. Heat Mass Transf.* 56 (1-2) (2013) 606–624.
- [21] A.K. Shukla, A. Dewan, Openfoam based les of slot jet impingement heat transfer at low nozzle to plate spacing using four SGS models, *Heat Mass Transf.* 55 (3) (2019) 911–931.
- [22] H. Li, N. Anand, Y.A. Hassan, T. Nguyen, Large eddy simulations of the turbulent flows of twin parallel jets, *Int. J. Heat Mass Transf.* 129 (2019) 1263–1273.
- [23] A. Pal, K. Anupindi, Y. Delorme, N. Ghaisas, D.A. Shetty, S.H. Frankel, Large eddy simulation of transitional flow in an idealized stenotic blood vessel: evaluation of subgrid scale models, *J. Biomech. Eng.* 136 (7) (2014) 071009.
- [24] P. Lampitella, R. Mereu, E. Colombo, F. Inzoli, Large eddy simulation of the flow and heat transfer in a matrix of cubes, in: ASME 2014 4th Joint US-European Fluids Engineering Division Summer Meeting collocated with the ASME 2014 12th International Conference on Nanochannels, Microchannels, and Minichannels, American Society of Mechanical Engineers, 2014. V01AT09A013–V01AT09A013
- [25] H.G. Weller, G. Tabor, H. Jasak, C. Fureby, A tensorial approach to computational continuum mechanics using object-oriented techniques, *Comput. Phys.* 12 (6) (1998) 620–631.
- [26] OpenFOAM documentation, <http://www.openfoam.org/>, Version 5.0.
- [27] J. Smagorinsky, General circulation experiments with the primitive equations: I. The basic experiment, *Month. Weather Rev.* 91 (3) (1963) 99–164.
- [28] A. Yoshizawa, Bridging between eddy-viscosity-type and second-order turbulence models through a two-scale turbulence theory, *Phys. Rev. E* 48 (1) (1993) 273.
- [29] F. Nicoud, F. Ducros, Subgrid-scale stress modelling based on the square of the velocity gradient tensor, *Flow Turbul. Combust.* 62 (3) (1999) 183–200.
- [30] W.-W. Kim, S. Menon, A new dynamic one-equation subgrid-scale model for large eddy simulations, in: 33rd Aerospace Sciences Meeting and Exhibit, 1995, p. 356.
- [31] M. Germano, U. Piomelli, P. Moin, W.H. Cabot, A dynamic subgrid-scale eddy viscosity model, *Phys. Fluid* 3 (7) (1991) 1760–1765.
- [32] D.K. Lilly, A proposed modification of the Germano subgrid-scale closure method, *Phys. Fluids* 4 (3) (1992) 633–635.
- [33] B. Kader, A. Yaglom, Heat and mass transfer laws for fully turbulent wall flows, *Int. J. Heat Mass Transf.* 15 (12) (1972) 2329–2351.
- [34] I. Celik, M. Klein, J. Janicka, Assessment measures for engineering les applications, *J. Fluids Eng.* 131 (3) (2009) 031102.
- [35] B.J. Geurts, J. Fröhlich, A framework for predicting accuracy limitations in large-eddy simulation, *Phys. Fluids* 14 (6) (2002) L41–L44.
- [36] I. Wygnanski, Y. Katz, E. Horev, On the applicability of various scaling laws to the turbulent wall jet, *J. Fluid Mech.* 234 (1992) 669–690.